

Two-photon absorption and optical limiting in 7-diethylamino-4-methyl coumarin

Shradha Lakhera^a, Kamal Devlal^a, Meenakshi Rana^{a,*}, N. Kanagathara^b, A. Dhanusha^c, T.C. Sabari Girisun^c, Shruti Sharma^d, Papiya Chowdhury^d

^a Department of Physics, School of Sciences, Uttarakhand Open University, Haldwani 263139, Uttarakhand, India

^b Department of Physics, Saveetha School of Engineering, Saveetha Institute of Medical and Technical Sciences, Thandalam, Chennai 602105, Tamil Nadu, India

^c Nanophotonics Laboratory, Department of Physics, Bharathidasan University, Tiruchirappalli, Tamil Nadu 620024, India

^d Department of Physics and Materials Science and Engineering, Jaypee Institute of Information Technology, Noida 201309, Uttar Pradesh, India

ARTICLE INFO

Keywords:

Molecular electrostatic potential
Mulliken charges
Nonlinear optical
7-diethylamino-4-methyl coumarin

ABSTRACT

The combined experimental and computational spectroscopic calculations were performed to analyze the nonlinear optical property of 7-diethylamino-4-methylcoumarin. The band gap was measured in ten different solvents and found very favorable in dimethyl formamide. The molecular electrostatic potential surface and Hirshfeld's surfaces were used to determine the reactive sites of the title molecule. Intramolecular interactions were accounted by Mulliken and natural charge distribution, Fukui functions, and fingerprint plots. The electronic transitions were studied by experimental and computed absorption and photoluminescence spectra. Infrared spectroscopy combined with DFT calculation was used to confirm the molecular vibrations related to the chemically active functional groups. The high value of hyperpolarizability showed the enhanced nonlinear optical behavior of the molecule. The Z-Scan plots gave a valley-like shape showing the occurrence of the reverse saturable absorption and the theoretical fit revealed the occurrence of two-photon absorption and the potential application of the molecule to be used for optical limiting applications.

1. Introduction

When we talk about the phenomenon and experiments of intense field, lasers are the most common and significant devices that come into the discussion. The invention of lasers has led to tremendous development in the field of high-intensity fields. Non-linear Optics (NLO) is a major subject that deals with the high-intensity field [1–3]. NLO materials have gained popularity due to their potential applications like telecommunications, optical limiting, data storage, optical sensing, imaging and holography, and many more [4–6]. In the past few decades, researchers have designed and introduced numerous crystalline structures with the help of organic systems, hybrid systems, dyes, polymers, hydrocarbons, quantum dots, aromatic compounds, fatty alcohols, conjugated systems, plant phytochemicals, and many more [7–10]. One of these systems is dyes that have grown a keen interest in researchers. The specific functional groups present in organic dyes majorly impart in inducing the stability and high chemical reactivity of the dyes [11,12]. The production of free charge clouds from electron-excess parts and the involvement of the cloud by the electron-deficient parts of the dyes make

them significantly high in chemical reactivity giving rise to the large induced dipole moment of the systems [13]. Moreover, the thorough charge interactions are optimally supported by the conjugation of the dyes. Therefore, dyes have attained special importance in the field of NLO materials.

Coumarin is one such dye that has numerous derivatives and conjugated structures employed as NLO materials [14]. Coumarin dyes have broad absorption around 400–450 nm with good inter and intramolecular interactions [15]. Many derivatives of coumarin were used for the formation of the Donor- π -Acceptor bridge molecule for the formation of the path for charge cloud to induce intramolecular charge transfer (ICT) [16]. Nitesh N. Ayare and the team worked on the thiophene-based azo-linked D- π -A coumarin dyes and designed four different isomers with the resonating structures of the dye [17]. In their study, all four structures gave a band gap between 2.5 and 2.9 eV with the property of saturable absorption and good thermal stability. The NLO responses of carbazole-coumarin-based chalcones and D- π -A- π -D type structures with carbazole as donor substituted with N-alkyl chain with carboxylic acid end group as acceptors were studied in detail in a

* Corresponding author.

E-mail address: mrana@uou.ac.in (M. Rana).

<https://doi.org/10.1016/j.jphotochem.2023.115216>

Received 22 August 2023; Received in revised form 21 September 2023; Accepted 1 October 2023

Available online 5 October 2023

1010-6030/© 2023 Elsevier B.V. All rights reserved.

study by M. Rajeshirke and the team [18]. These carbazole-coumarin-based chalcones gave a promising band gap between 2.5 and 3.3 eV with an excellent two-photon absorption phenomenon. Sharafudeen and the team worked on NLO characteristics of coumarin derivatives [3-[(2E)-3-phenylprop-2-enoyl]-2H-chromen-2-one and 3-[(2E)-3-[4-(dimethylamino)phenyl]prop-2-enoyl]-2H-chromen-2-one doped in a polymer matrix of polymethylmethacrylate using Z-scan and hyperpolarizability analysis [19]. The results of the Z-scan established reverse saturable absorption due to excited state absorption in the samples. This article also reports the enhancement of third-order nonlinearity due to the suitable band gap and electronic nature of nonlinearity. The identification of NLO activity of novel coumarin-benzene sulfonyl hydrazide hybrids was done by K.N. Chethan Prathap and N.K. Lokanath [20]. These hybrid structures have a band gap around 4.2 eV and the absorption peak lies in the UV region of 250–350 nm wavelength. Thermogravimetric analysis showed that the compounds are thermally stable up to a temperature of 190 °C. M. Raikwar and the team worked on four new D- π -A- π -D hybrid dyes containing coumarin as a major donor together with carbazole and triphenylamine as an auxiliary donor having dicyanovinylene as a common acceptor [21]. These hybrids show reverse saturable kind of behavior and hence give optical limiting values.

Thus, from the studies reported in the literature, coumarin dyes can be considered promising candidates for NLO application in material science. Herein, taking into consideration all the above-mentioned studies the present study reports the NLO activity and the optical limiting applications of the coumarin 7-diethylamino-4-methylcoumarin (7DMC) by computational and theoretical approaches. As the occurrence of the ICT suggests the NLO activity of the compound and the compounds having some donor–acceptor moieties in their structures have a probability of having NLO responses. The title compound 7DMC also has nitrogen and oxygen atoms. The oxygen atoms act as perfect electron-withdrawing and the nitrogen acts as electron-donating moieties. These atoms play a vital role in increasing the intramolecular interactions leading to high chemical reactivity of 7DMC. In this context, the availability of electron-deficient and electron-excessive moieties makes 7DMC a potential candidate for studying its NLO applications. Another reason for the consideration of the 7DMC for this study is the location of the donor or acceptor groups that fall near enough to give the large possibility of the charge transfer. Recently, a study was reported in which Nadia Arif and the team proposed two coumarin-based pyranochromene derivatives namely 2-amino-8-methyl-5-oxo-4-[2-(2-oxo-2H-chromen-3-ylmethoxy)-phenyl]-4H,5H-pyrano[3,2-c]chromene-3-carbonitrile and 2-amino-8-methyl-5-oxo-4-[2-(2-oxo-2H-chromen-3-ylmethoxy)-phenyl]-4H,5H-pyrano[3,2-c]chromene-3-carboxylic acid methyl ester which were employed for the NLO applications [22]. These structures were theoretically shown to have distinguished values of NLO parameters but because of having large aromatic clusters in the structures, the donor–acceptor moieties were situated at a significant distance from each other. Similarly, four 3-(p-nitrophenyl) Coumarin derivatives namely 3-(p-nitrophenyl) iminocoumarin, 3-(p-nitrophenyl) coumarin, 8-Methoxy-3-(p-nitrophenyl)iminocoumarin, and 8-Methoxy-3-(p-nitrophenyl)coumarin were studied by N. B. Azaza and the team [23]. The donor–acceptor groups in these derivatives were also observed to be bonded to the opposite positions of a benzene ring and these derivatives were used for second harmonics generation [23]. The Density functional theory was used for the computational calculations. The UV–Vis, FT-IR, and Z-scan experiments were performed for the validation of the NLO behavior of 7DMC.

2. Materials and methods

2.1. Computational details

The PDB structure of 7DMC was taken from PubChem (CID:7050) (<https://pubchem.ncbi.nlm.nih.gov/>). Gaussian tools (<https://gaussian.com>)

were used for all the quantum chemical calculations and the visualizations were done using the Gauss view program (<https://gaussian.com/gaussview6/>) [24]. The geometry of 7DMC was optimized using a B3LYP basis set with 6–311++G(d,p) set of functions where (d,p) are the polarization functions and ++ denotes the addition of a set of diffused s-functions and diffused p-functions to all the heavy atoms (say carbon, nitrogen, and oxygen in title molecule) [25]. Solvents like acetonitrile, dimethyl sulfoxide (DMSO), methanol, acetone, dichloromethane, dichloroethane, tetrahydrofuran (THF), aniline and dimethylformamide (DMF) were used for reporting the solvent effect. The B3LYP/6–311++G(d,p) set of hybrid functions were used for calculating the ground state geometry optimization. In DFT, the integral equation formalism-polarizable continuum model (IEFPCM) is suitable for solvent effect and thus it was used to create the solute cavity with the self-consistent reaction field (SCRF) method. The structure optimization was done in 10 different solvents to select the best solvent that can be further used for experiments. The optimized geometry was further employed for the comparison between the Mulliken charges and natural charges. The density of states (DOS) spectra was obtained by Gauss Sum software [26]. The settlement of the highest occupied and lowest unoccupied molecular orbitals (HOMO-LUMO) was reported by DOS spectra. Further, the energies corresponding to the HOMO-LUMO were employed for the calculations of the reactivity parameters using Koopman's equations [27,28]. The time-dependent self-consistency field (TD-SCF) was used to calculate the absorption and emission spectra of 7DMC. The polar calculations were performed to obtain the vibrational spectra. The vibrations of the reactive bonds were studied and reported by the simulated FT-IR spectra. All the spectroscopic characterizations were done experimentally as well as computationally and were compared. Crystal explorer packages (<https://crystalexplorer.net/>) were used for the analysis of Hirshfeld's surfaces and 2-D fingerprint plots were visualized to study the interactions between the reactive moieties [29]. Additionally, the enrichment ratios of the intramolecular contacts were also calculated to estimate the propensity of two chemical species to be in contact. The hyperpolarizability parameters for 7DMC were calculated to account for the quantitative nature of NLO activity.

2.2. Experimental details

7DMC (C₁₄H₁₇NO₂) (D5730;>99.5 %) and dimethyl formamide (DMF) were purchased from TCI chemicals (<https://www.tcichemicals.com/IN/en/search/?text=7-Diethylamino-4-methylcoumarin>) and was used as it is. The spectroscopic characterization absorption and emission were performed for 7DMC in the selected solvent. The 7DMC solution of concentration 5×10^{-3} M was prepared and used for the spectral characterizations of absorption, photoluminescence, and Fourier-transform infrared spectroscopy (FT-IR). The same UV, PL, and FT-IR spectroscopes that were used in the previously done study were used for the present study [30]. The band gap (E_g) was calculated using the experimentally obtained absorption data. Tauc's plot was drawn with the help of Mott and Davis's relationship given below [31].

$$(ah\nu)^{\gamma} = A(h\nu - E_g) \quad (1)$$

The NLO behavior of the 7DMC and third-order absorption coefficient was predicted by performing the Z-scan spectroscopy. The intensity-dependent open aperture Z-scan was performed using a 532 nm nano-pulsed Nd: YAG laser beam of 17 μ m waist and 10 Hz frequency focused by the lens of 15 cm focal length. The solution of concentration 2 mg/cm³ was prepared using DMF as solvent. The data obtained were fitted theoretically and the normalized transmittance was computed by Sheik-Bahae formalism mentioned below:

$$\frac{dI}{dZ} = \left[\frac{\alpha_0}{1 + \frac{I}{I_s}} + \beta I \right] I \quad (2)$$

where α_0 is unsaturated linear absorption at the excitation, I is input intensity laser, I_s is saturation intensity, $\beta\beta$ is the effective coefficient of two-photon absorption (nonlinear absorption coefficient), and Z is the sample propagation distance.

In the Z-scan setup, P and P_0 were the values of the output and input power. These values were used to calculate the value of linear transmittance (L_T):

$$L_T = \frac{P}{P_0} \quad (3)$$

Further, the L_T and the sample thickness ($L = 1$ mm) were used to calculate the linear absorption coefficient (α_0) was computed using L_T and sample thickness (1 mm) by equation

$$\alpha_0 = -\left(\frac{1}{L}\right) \ln\left(\frac{P}{P_0}\right) \quad (4)$$

3. Results and discussion

3.1. Solvent effect

The present study targets the establishment of the NLO activity of 7DMC. Coumarin derivative 7DMC is experimentally soluble in acetonitrile, DMSO, methanol, acetone, dichloromethane, dichloroethane, THF, aniline, and DMF. To see the best solvent for the experimental purpose, the structure optimizations of 7DMC were carried out in all the mentioned solvents. The energies corresponding to HOMO, and LUMO in all the ten solvents were listed in SD 1. The band gap was calculated by the difference between LUMO and HOMO energy [32]. For the validation of the solvent selection, the dipole moment and band gap of 7DMC in all the selected solvents were compared (Fig. 1). The band gap and dipole moment analysis done in different solvents suggests that DMF (band gap 3.691 eV and dipole moment 11.12 Debye) and DMSO (band gap 3.689 eV and dipole moment 11.16 Debye) are the better solvents for experimental usage. However, DMF has a lower boiling point (153 °C) as compared to DMSO (189 °C) and thus has higher chances of being evaporated easily as compared to DMSO during the crystallizing process. As the study targets the NLO responses of 7DMC and its applications, it can be further used as a basis for crystal growth of 7DMC and in further NLO applications like second harmonic generation. Thus, keeping in mind, the futuristic applications of the reported work DMF is taken as solvent for spectroscopic studies mentioned in the article.

3.2. Structural and charge analysis

The optimized geometry of 7DMC has C1 point group geometry with no imaginary frequencies (Fig. 2). The non-centrosymmetric geometry of 7DMC gave the dipole moment of 11.25 Debye. The bond lengths of the optimized geometry of 7DMC were analyzed and listed in SD 2. The 7DMC has one carbonyl group 2O=17C one oxygen 1O attached to one benzene and two ethyl groups attached to the 3N atom. The carbonyl

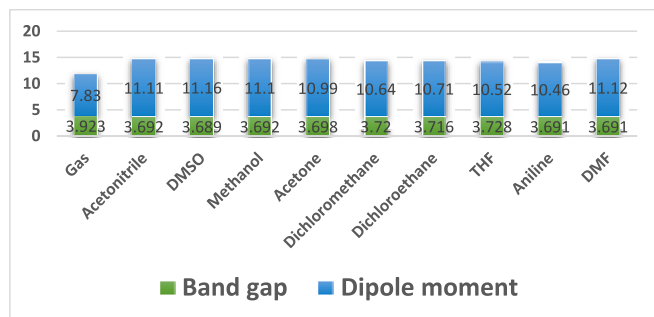


Fig. 1. Comparison of the band gap and dipole moment of 7DMC in different solvents (band gap is in eV and dipole moment is in Debye).

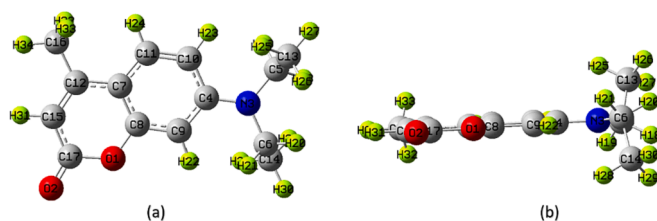


Fig. 2. (a) Optimized structure of 7DMC in DMF from the front side, (b) side view of 7DMC showing non-planer geometry of 7DMC.

being highly electronegative makes the low lengths bond with the benzene ring. On the other hand, nitrogen being highly electropositive makes bonds with high bond lengths with the benzene as well as the ethyl groups. The bond length of 2O=17C was observed as 1.22 Å which was the minimum among the other bonds. The nitrogen atom was attached to benzene and ethyl groups with 3N-4C, 3N-6C, and 3N-5C with bond lengths of 1.38 Å, 1.47 Å, and 1.47 Å respectively. The bond lengths of these bonds were observed to be higher than the bonds associated with the carbonyl. Additionally, the bonds between the carbon atoms of the ethyl chains 6C-14C and 5C-13C were observed to have the highest bond length of 1.53 Å each. The higher bond lengths were supposed to be easily dissociated and generate the charge cloud that would create the probability of intramolecular interactions. These intramolecular interactions were demonstrated by the Mulliken and natural charge distribution (Fig. 3). The natural charges are more accurate, reliable, electron density-dependent, and is helpful in describing the electron density. Mulliken charge distribution, on the other hand, is the fastest way to compute charge distribution and is basis set dependent. The natural and mulliken charges were compared to validate the selection of the considered basis set as well as all the parameters derived using the basis set. Oxygen atoms have a negative charge contribution towards the total charge of 7DMC whereas the 4C atom that bounds the nitrogen atom to the benzene ring imparts positively to the total charge contribution of the molecule (SD 3). Also, the 17C atom of the carbonyl group acts as a highly positive charge contributor to 7DMC. This variation in the charge distribution supports the generation of the charge cloud from the 3N and accepting nature of the carbonyl group and reflects the possibility of the occurrence of the charge cloud in 7DMC.

3.3. Potential Surfaces, hirshfeld's and fingerprint plots analysis

The MEP surface illustrated in Fig. 4 (a) was used to locate the nucleophilic and electrophilic moieties within 7DMC. The lightly visible blue color over the 3 N atom represents the electron-donating part and the red color area over the 2O=17C bond and O atom represents the electron-withdrawing part of 7DMC. The location of the nucleophilic and electrophilic part in the MEP surface reveals the dislocation of the charge cloud from 3 N atoms towards the O atoms. The counter plots shown in Fig. 4(b) also support the interpretation of the MEP surface. The highly accumulated field lines near the C=O bond and O atom show the accumulation of the charge cloud. The intermolecular interactions were predicted using Hirshfeld surfaces. The d_i and d_e represents the distance between the surface and the nearest atom outside and inside respectively (Fig. 4(c) and 4(d)). The red spots over the alkyl fragments connected to the N atom reveal that the alkyl parts are the farthest from the Hirshfeld and hardly contribute to the intermolecular interactions. On the other hand, the d_e surface indicates the 2O=17C bond and 3 N atoms as the nearest part to the surface. The d_{norm} is the normalized contact distance of the molecule from the surface (Fig. 4 (e)). The red spots in the d_{norm} were located over the O atoms of the 2O=17C bond and N atoms. This shows that the O and N atoms are the nearest ones to the Hirshfeld surface and are the active regions for inducing the charge interactions. The shape index (Fig. 4(f)), curvedness (Fig. 4(g)), and fragment path (Fig. 4(h)) were depicted in ranges ± 1.00 Å, ± 0.400 Å,

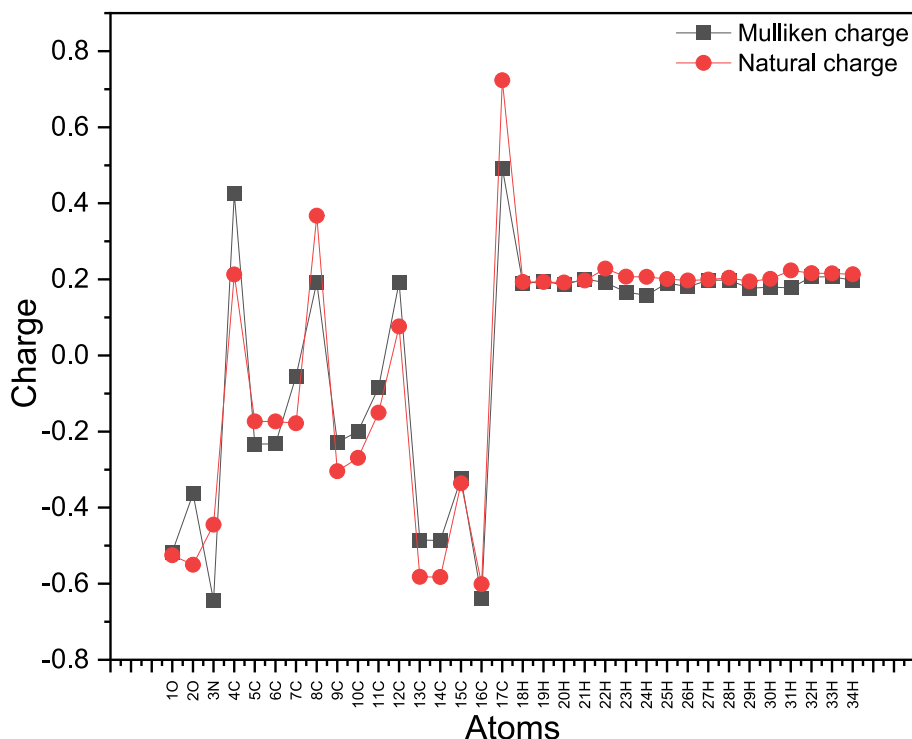


Fig. 3. Comparison of the Mulliken charges and the natural charges of the atoms of 7DMC in DMF.

and 0.00–13.00 Å respectively. These surfaces were in better agreement with the d_{norm} surface. The curvedness mapping was observed over the 2O=17C and 3 N atoms. The internal curves and the external curves over 3 N and 2O=17C bonds show the convex-concave intermolecular interactions between both atoms. The inflection over the 3 N and 2O=17C bonds reveals the face-to-face π -stack contacts between both moieties. The fragment patches mapping colors help in the identification of the closest neighbor coordination environment of a molecule for both compounds [33]. All the surfaces support the donor and acceptor parts of 7DMC and confirm the intramolecular interactions within 7DMC.

The 2-D fingerprint plots traced for the interatomic interactions of 7DMC are illustrated in Fig. 5. The fingerprint plots gave the percentage of interatomic interactions of 7DMC. Fingerprint plots of 7DMC have five main peaks representing the interatomic interactions among all the atoms and the total molecular surface. The highest interatomic interactions of 49.6 % were obtained for H...H interactions. The overall Hirshfeld's surface has 76.9 % interactions with H and H atoms have 72.3 % interactions with the overall Hirshfeld's surface. These interactions gave the central and the most-broad peak in the fingerprint. The hydrogen bond interactions were found to have major interatomic interactions. After hydrogen bond interactions, the H...C and C...H interactions impart 12.4 % and 14.1 % respectively. The H...C interactions were mainly responsible for the uppermost peak of the fingerprint. The oxygen atoms of the carbonyl group interact with hydrogen atoms with H...O/O...H of 9.9 and 12.8 %. These interactions reflected the second uppermost peak of the fingerprint. The fingerprint plots and the Hirshfeld surfaces confirm the occurrence of the intramolecular interactions within the 7DMC.

3.4. Local reactivity descriptors: Fukui functions analysis

Fukui functions are the local reactivity descriptors that help in the identification of the chemical moieties with excess and deficient charge density after the modification of the electrons [34,35]. The Fukui functions are represented by N+1 and N-1 electronic states and are expressed as [36]:

$$f^+ = q_N - q_{N+1}; \text{favourable for nucleophilic attack}$$

$$f^- = q_{N-1} - q_N; \text{favourable for electrophilic attack}$$

The condensed dual Fukui descriptor is defined as $\Delta f = f^+ - f^-$ (Table 1). The positive value of Δf ($\Delta f > 0$) is favored for nucleophilic attack and the negative value of Δf ($\Delta f < 0$) is favored for the electrophilic attack [37]. The MEP surface validated the charge transfer from nitrogen toward oxygen atoms. Following this pattern, the Fukui functions were calculated for 1O, 2O, 17C, 3N, 4C, 5C, and 6C. The Fukui function Δf is calculated using plus-one and minus-one charge values obtained in the calculations. From the Fukui function values, negative values of Δf for 1O, 2O, and 17C were calculated showing their electrophilic nature, and the positive values for 3N, 4C, and 5C showed their nucleophilic nature. Thus, the Fukui functions gave better support for the prediction of the electron-donating and electron-withdrawing parts of the 7DMC molecule.

3.5. Global reactivity descriptors: Reactivity parameters

The molecular mechanism of the reactivity of the 7DMC was explained by the global reactivity parameters. These parameters were calculated using Koopman's set of equations [38,39]. The energies of the frontier molecular orbitals HOMO and LUMO were used for calculating the parameters (Table 2) [40]. The ΔE was calculated as 3.691 eV. This value was smaller than the ΔE of reference material Urea (7.43 eV) [41]. IP is the property of the molecule to donate the electron charge cloud and the high value of IP (5.557 eV) shows the easy charge release from 7DMC for the bond formation. The charge-withdrawing activity of the molecule is measured by EA. The low value of EA (1.881 eV) shows that low energy is required for withdrawing the charge cloud from the donating moiety. CP is the energy that is released during the dissociation of the charge cloud from the donating to withdrawing atoms of the molecule [42]. The more the CP is negative, the less energy is required by the molecule to be chemically reactive [43]. The CP is the property that accounts for the chemical activity of the material toward the intramolecular interactions and its high value i.e., -3.729 eV justifies

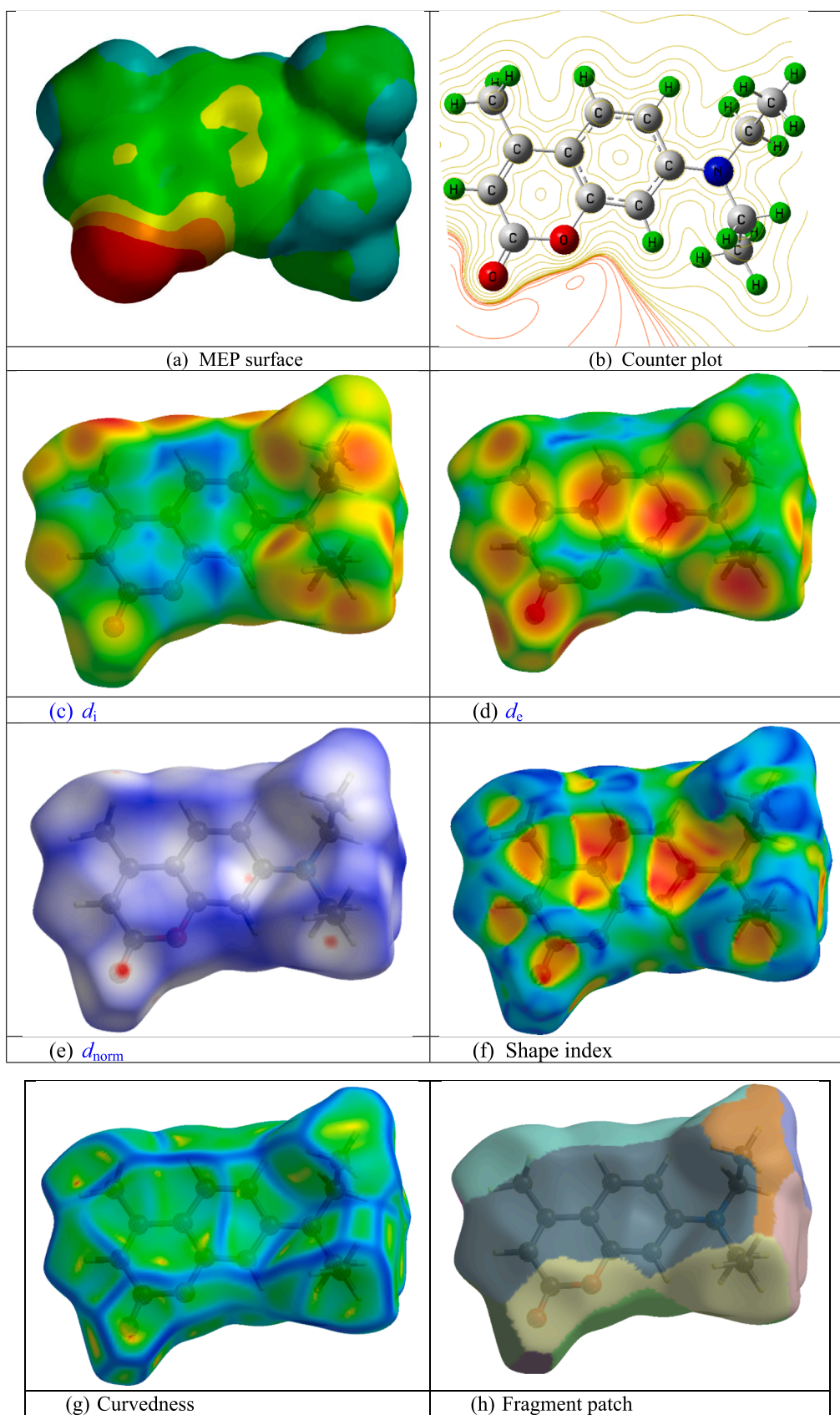


Fig. 4. Molecular electrostatic potential surface and Hirshfeld surfaces of 7DMC in DMF.

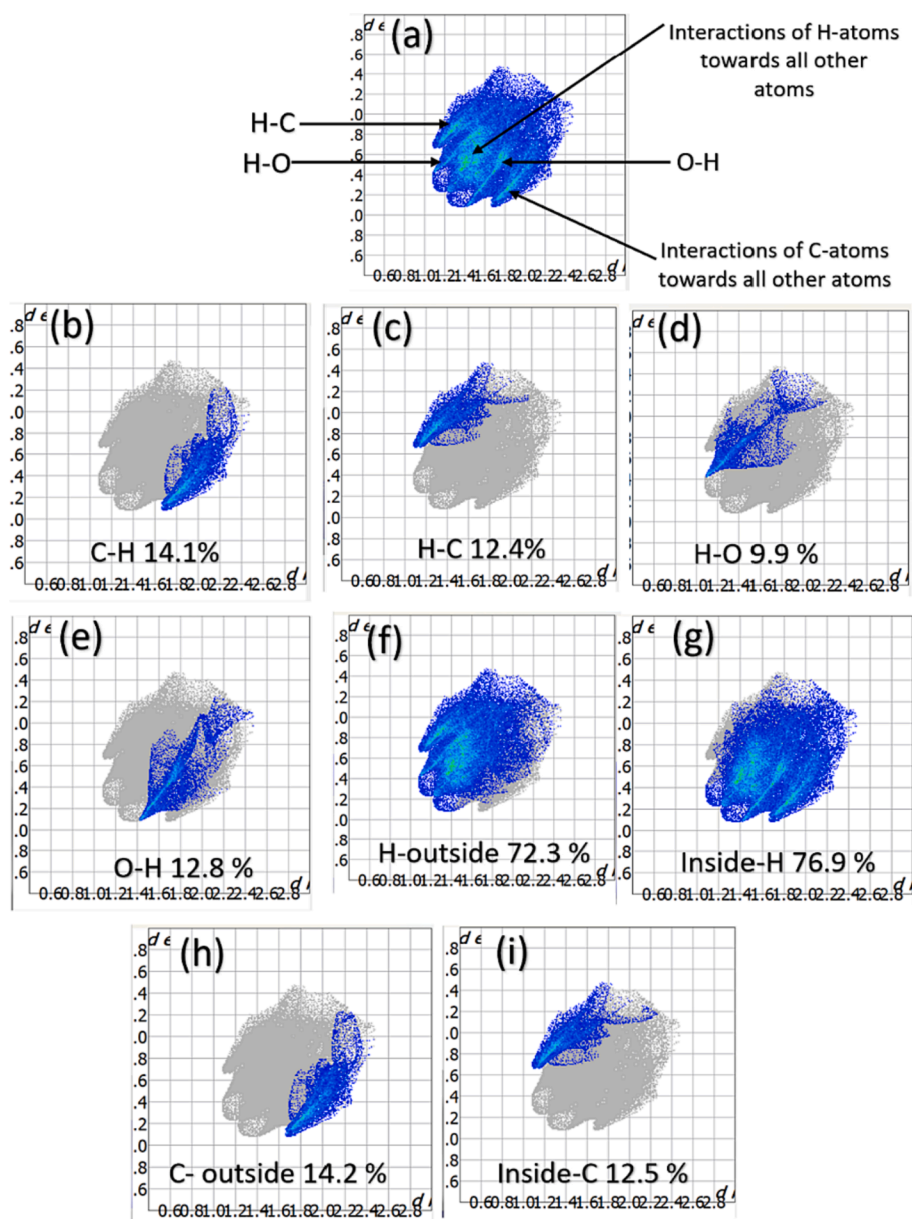


Fig. 5. 2D fingerprint plots of 7DMC molecule in DMF showing the percentage of the interaction of interatomic bonds.

Table 1
Calculated Fukui functions for the reactive atoms of 7DMC in DMF.

Fukui functions Atoms	Plus-one charge			Minus-one charge		
	f^+	f	Δf	f^+	f	Δf
1O	0	0.0021	-0.0021	0	0.0001	-0.0001
2O	0	0.9666	-0.9666	0	0	0
17C	0	0.0118	-0.0118	0	0	0
3N	0.0076	0	0.0076	0.0073	0	0.0073
4C	0.5502	0.0001	0.5501	0.4761	0	0.4761
5C	0.0002	0	0.0002	0.0001	0	0.0001
6C	0.0002	0	0.0002	0.0002	0	0.0002

7DMC as the chemically reactive agent. Chemical hardness is the extent to which the molecule resists deformation during chemical reactions. Due to the high value of η (1.848 eV) and low value of S (0.541 eV⁻¹), 7DMC can be considered a chemically stable molecule that stiffly undergoes chemical reactions. The electrophilicity index (ω) is the

Table 2
Values of global reactivity parameters of 7DMC in DMF.

S No.	Molecular property	7DMC
1.	E_{HOMO}	-5.577
2.	E_{LUMO}	-1.881
3.	Energy gap (ΔE)	3.691
4.	Ionization potential (IP)	5.577
5.	Electron affinity (EA)	1.881
6.	Chemical potential (CP)	-3.729
7.	Electronegativity (χ)	3.729
8.	Hardness (η)	1.848
9.	Softness (S)	0.541
10.	Electrophilicity index (ω)	3.508
11.	Electron accepting power (ω^+)	2.128
12.	Electron donating power (ω^-)	5.857

quantitative parameter that measures the ability of the molecule to take up electrons and is dependent on the IP and η of the molecule [44]. The higher value of IP and lower value of η result in the high value of ω . The

ω^- was found higher than the ω^+ . This ultimately draws the electron-donating activity of the 7DMC molecule. The values of all the global reactivity parameters show that 7DMC is an immense chemically hard and stable molecule.

3.6. Electronic transitions analysis

The UV-Vis spectrum of 7DMC in DMF was measured experimentally as well as computationally (Fig. 6 (a) and (b)). The details of all the absorptive and emissive transitions have been mentioned in SD 4. The broad experimental absorption band between 300 and 450 nm with a peak at 370 nm was observed. The Tauc plot was also plotted for 7DMC to depict the band gap of the title molecule (Fig. 6 (c)). The graph plotted between $(\alpha h\nu)^2$ and energy gave an experimental band gap of 3.68 eV. The experimentally obtained band gap was nearly equal to the band gap obtained by the frontier molecular orbitals (3.691 eV). The comparison was enough to justify the computational results. Similar to the experimental band, a broad absorption band was computationally obtained between 250 and 450 nm. The S_0 to S_1 transition with wavelength 341 nm and excitation energy 3.6 eV was obtained. A shoulder peak was also observed near 340 nm in experimental absorption spectra. Some electronic transitions were expected near the shoulder. This was confirmed by the computed spectra where S_0 to S_2 and S_0 to S_3 transitions with 285 nm and 280 nm wavelengths were observed. Therefore, the $\pi-\pi^*$ transitions are seen as most likely to be responsible for the electronic absorption spectra of 7DMC in this range. The emission spectra were also obtained computationally and experimentally. The broad experimental emission was obtained between 350 and 500 nm with a peak at 436 nm. A similar kind of broad emission spectra was obtained computationally between 300 and 400 nm. The emissive transition S_0 to S_1 with an excitation energy of 3.3 eV and oscillator strength of 0.3666 was

responsible for the peak of the computed emission spectra. The emission spectra in both experimental and computational fall at the higher wavelengths as compared to the wavelength of absorption spectra and are thus found shifted. This validated the computational results generated by DFT. The UV-Vis spectra verified the occurrence of the electronic transitions. Thus, the molecular orbital surfaces were also plotted to support the electronic transitions. For this, the HOMO-LUMO surfaces were located and illustrated in Fig. 6 (d). The plotted HOMO-LUMO surfaces were shown in red and green surfaces. The negative charge contributory atoms were covered by red surfaces and the positive charge contributory atoms were surrounded by green surfaces [45]. The major and large orbital surfaces were seen to cover the nitrogen atom and nearby alkyl chains. The red color surface over the nitrogen in HOMO is shifted to the green color surface over the nitrogen in LUMO. That red color surface was observed over the oxygen atoms with enhanced size. This shifting of the molecular surface from nitrogen towards the oxygen atoms might be due to the electronegativity of the nitrogen and the high electronegativity of the oxygen atoms. The delocalization of these orbital surfaces shows the occurrence of ICT between the nitrogen and oxygen atoms.

3.7. Vibrational analysis

The vibrational modes were obtained experimentally as well as theoretically to get an understanding of the vibrating bonds of 7DMC (Fig. 7). In the range 500 to 1000 cm^{-1} , the bending of C-H bonds was observed, and the symmetric (ν) and asymmetric stretching (α) of C-H bonds were observed between 2000 and 4000 cm^{-1} . The major vibrational peaks were observed between 1000 and 2000 cm^{-1} and details of the vibrational modes are listed in SD 5. The torsional bending (δ) of the C-N bonds and the $\nu_{\text{C-N}}$ modes peaks were observed at 1101, and 1177

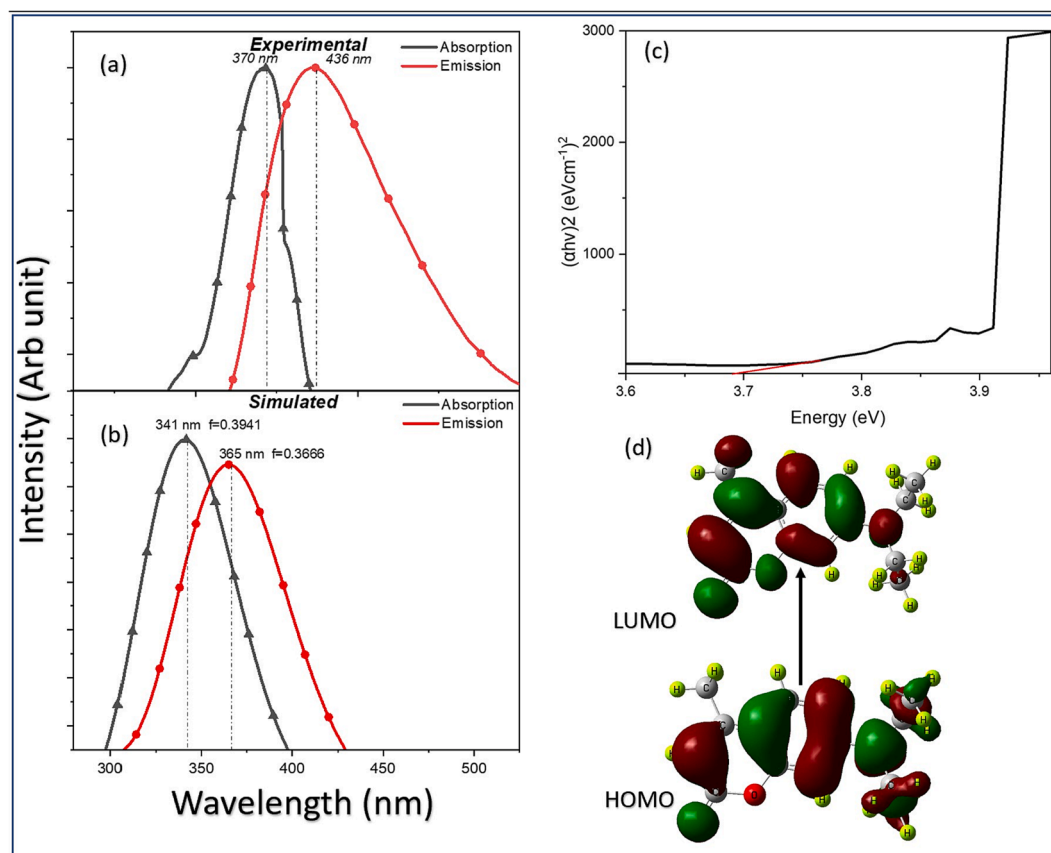


Fig. 6. (a) Experimental and (b) computed absorption and emission spectra of 7DMC in DMF, (c) Tauc plot for depicting the band gap of the 7DMC. (d) Location of the molecular orbitals surfaces over the 7DMC in DMF.

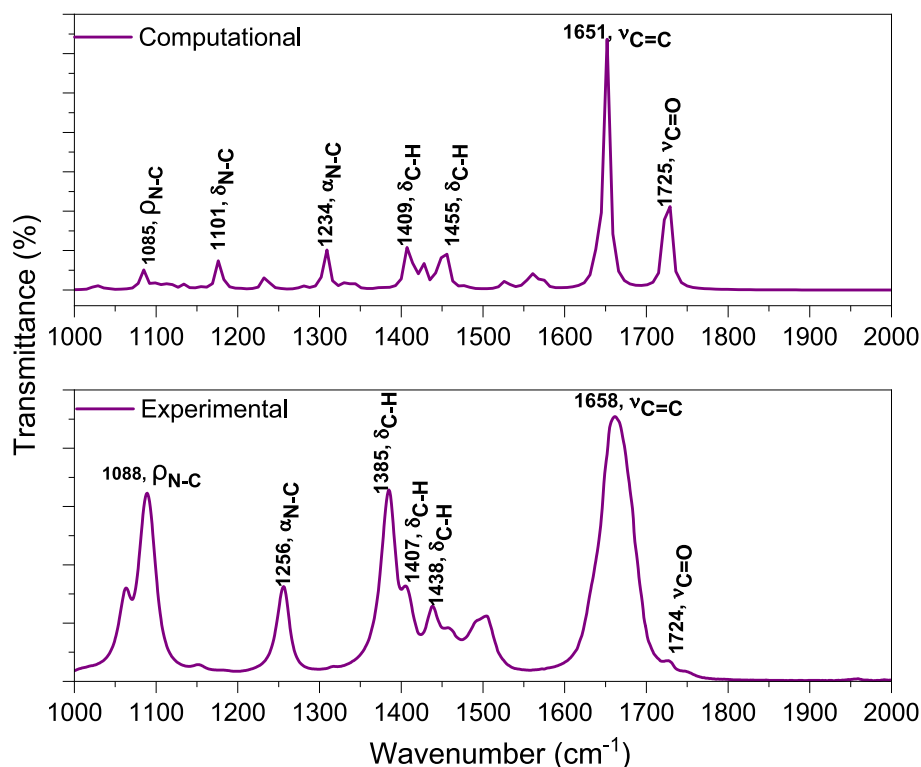


Fig. 7. Experimental and computed FT-IR spectra of 7DMC in DMF (Symmetric stretching- ν , asymmetric stretching- α , torsional bending in the plane (scissoring)- δ , rocking- ρ).

cm^{-1} respectively. Corresponding to the peak at 1101 cm^{-1} , an experimental peak at 1100 cm^{-1} was observed for the bending of the N-C vibration. The $\alpha_{\text{C-N}}$ was observed at 1234 cm^{-1} . The $\delta_{\text{C-H}}$ bonds corresponding to the alkyl chains attached to the nitrogen atom gave two major peaks at 1308 , 1409 , and 1445 cm^{-1} . Corresponding to these peaks, the $\delta_{\text{C-H}}$ modes were experimentally obtained at 1392 and 1412 cm^{-1} . The most-strong peak was observed for stretching of both the conjugated C=C bonds of the benzene ring at 1651 cm^{-1} . This mode has the highest IR intensity of 938 cm^{-1} . A similar $\nu_{\text{C=C}}$ mode with a prominent IR peak was experimentally observed at 1652 cm^{-1} . The carbonyl bond $17\text{C}=\text{O}$ was found to give a sharp stretching peak at 1725 cm^{-1} . Parallel to the $\nu_{\text{C=O}}$ experimental mode, a small hump of $\nu_{\text{C=O}}$ mode in the $\nu_{\text{C=C}}$ mode in experimental spectra was observed. Corresponding to two separate peaks of $\nu_{\text{C=C}}$ and $\nu_{\text{C=O}}$ in computational spectra, a broad peak of $\nu_{\text{C=C}}$ with a slight hump of $\nu_{\text{C=O}}$ in experimental spectra was observed. These modes were the ones among all the other FT-IR modes with the highest IR intensity. The experimental and computed FT-IR spectra were found to give similar kind of behavior. Computationally, the observed modes give peaks in IR spectra having high values of Raman intensity. Thus, high Raman and FT-IR intensity corresponds to the high polarizability of the 7DMC molecule [46]. Therefore, the title molecule is expected to have high polarizability and FT-IR spectra reflect the engagement of nitrogen and oxygen atoms in the ICT as the bonds related to these atoms gave peaks in FT-IR.

3.8. Hyperpolarizability analysis

Dipole polarizabilities are the quantitative parameters that explain the excellent NLO activity of the materials. NLO responses can be calculated in terms of their first and second-order hyperpolarizability values. The delocalization of the π -electrons and intramolecular interactions are the basis of the NLO responses of materials. The materials undergoing these properties have high values of first and second-order hyperpolarizabilities. Following equations (5) to (8), the total

isotropic polarizability (α_{total}), anisotropic polarizability ($\Delta\alpha$), first-order hyperpolarizability (β_{total}), and second-order hyperpolarizability (γ_{total}) values along x , y and z -direction tensors [47,48].

$$\alpha_{\text{total}} = \frac{1}{2}(\alpha_{xx} + \alpha_{yy} + \alpha_{zz}) \quad (5)$$

$$\Delta\alpha = \frac{1}{\sqrt{2}}[(\alpha_{xx} - \alpha_{yy})^2 + (\alpha_{yy} - \alpha_{zz})^2 + (\alpha_{zz} - \alpha_{xx})^2 + 6\alpha_{xz}^2 + 6\alpha_{xy}^2 + 6\alpha_{yz}^2]^{\frac{1}{2}} \quad (6)$$

$$\beta_{\text{total}} = [(\beta_{xxx} + \beta_{yyy} + \beta_{zzz})^2 + (\beta_{yyy} + \beta_{zzz} + \beta_{yxx})^2 + (\beta_{zzz} + \beta_{xxx} + \beta_{zyy})^2]^{\frac{1}{2}} \quad (7)$$

$$\gamma_{\text{total}} = \frac{1}{5}[\gamma_{xxxx} + \gamma_{yyyy} + \gamma_{zzzz} + 2(\gamma_{xyxy} + \gamma_{yyzz} + \gamma_{xxzz})] \quad (8)$$

The values of all the tensor components of polarizability parameters were listed in SD 6. In NLO, polarization is not superimposed and splits into different orders of susceptibility. These parameters are the coefficients of the energy in the expansion of the polarization. The α_{total} and $\Delta\alpha$ are lower-order terms and reveal the optical linearity of the molecule and the higher-order coefficients (β_{total} and γ_{total}) are known to express the optical nonlinearity of the molecules. The value of α_{total} and $\Delta\alpha$ of 7DMC was calculated as 27.22×10^{-24} and 75.92×10^{-24} esu. These values were found to be four and twelve times higher than α_{total} (5.664×10^{-24} esu) and $\Delta\alpha$ (6.304×10^{-24} esu) of reference compound Urea [38]. These parameters reveal the optical linearity of 7DMC. The value of β_{total} of 7DMC was calculated as 18.46×10^{-30} esu which is twenty-three times higher than Urea (0.781×10^{-30} esu). Additionally, the FT-IR spectra the gave possibility of having a high polarizability of 7DMC, and this statement was well supported by the polarizability parameters. The high value of β_{total} of 7DMC reveals the potential characteristics of 7DMC as first-order NLO material. The second-order nonlinear susceptibility is defined as γ_{total} and accounts for the second-

order nonlinear optical activity of 7DMC. The value of γ_{total} for 7DMC was calculated as -1197×10^{-39} esu. The negative value of γ_{total} is due to the non-centrosymmetric structure 7DMC. The non-centrosymmetric structures allow 7DMC to behave as both second and third-order NLO materials. Therefore, the values of polarizability parameters established the second and third harmonic properties of the 7DMC molecule.

3.9. Z-scan and optical limiting (OL) analysis

The solution of 7DMC was prepared in the DMF with the linear absorption coefficient calculated as 2.876 cm^{-1} for executing the Z-scan experiment. The NLO activity and OL behavior of the 7DMC were experimentally studied by performing an open-aperture Z-scan experiment for three different intensities of $2.46 \times 10^{12} \text{ W/m}^2$, $3.69 \times 10^{12} \text{ W/m}^2$

m^2 , and $4.92 \times 10^{12} \text{ W/m}^2$. Values of the nonlinear absorption coefficient and optical limiting threshold for 7DMC are listed in SD 7 and the Z-scan patterns obtained are illustrated in Fig. 8. The valley-like structure symmetric to the focal axis ($Z = 0$) of the Z-scan pattern represents the occurrence of reverse saturable absorption (RSA). RSA is the process in which the transmittance of the sample decreases with the increase in the excitation laser power. Here the experimental data was fitted theoretically to identify the involved nonlinear absorption mechanism. As seen in Fig. 8, the best fit (solid line) obtained for the experimental data (scattered circles) arises for the two-photon absorption (2PA) equation. When the sample comes in contact with the green laser, there is the possibility of the occurrence of two different kinds of 2PA (genuine or sequential) [49]. The nature of 2PA cannot be predicted directly from the simple Z-Scan experiment. So, the intensity-dependent Z-scan

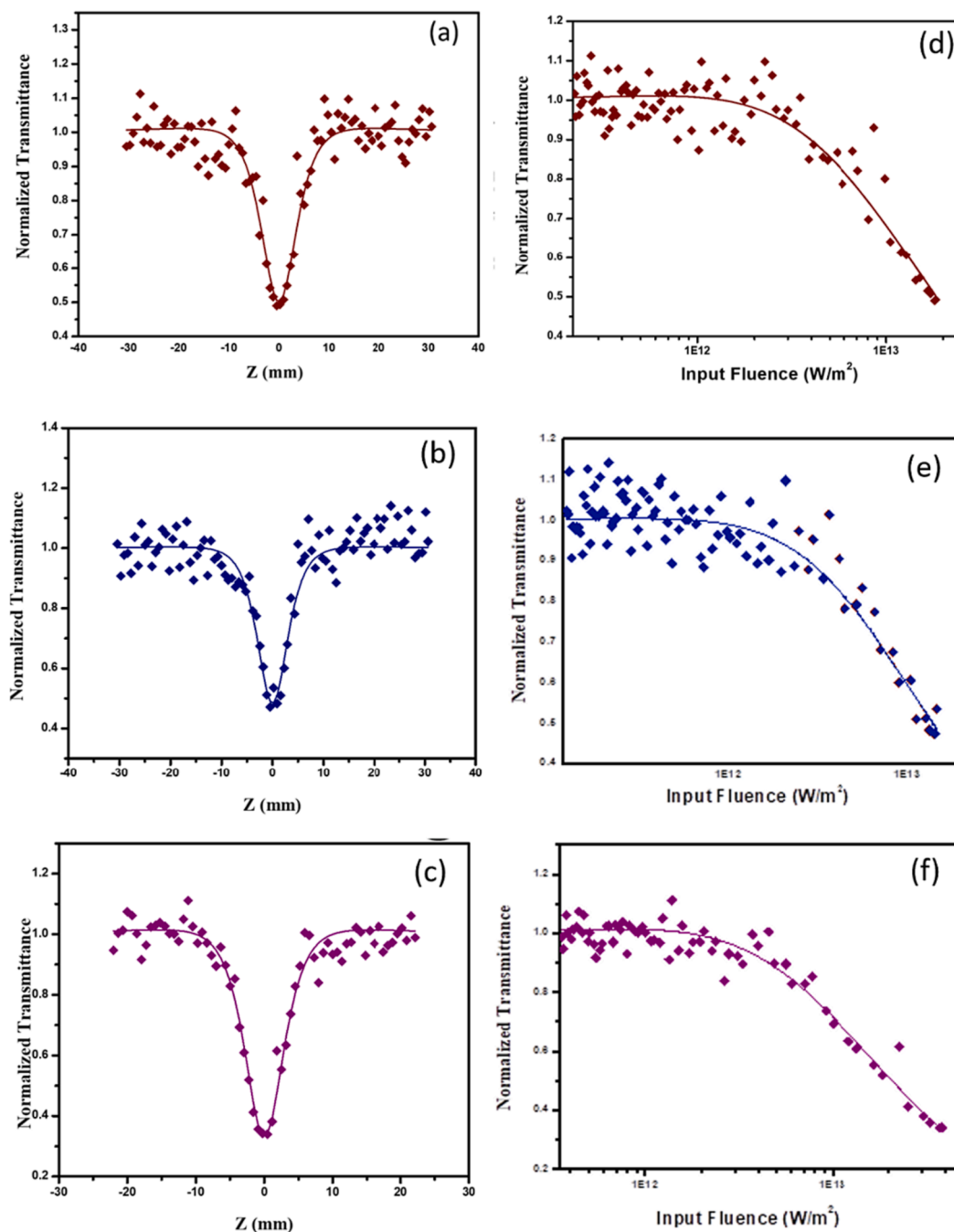


Fig. 8. Intensity-dependent Open-aperture Z-scan pattern of 7DMC in DMF using Nd:YAG nano pulsed laser (532 nm) for intensity (a) $2.46 \times 10^{12} \text{ W/m}^2$, (b) $3.69 \times 10^{12} \text{ W/m}^2$, and (c) $4.92 \times 10^{12} \text{ W/m}^2$. Optical limiting graph of 7DMC for intensity (a) $2.46 \times 10^{12} \text{ W/m}^2$, (b) $3.69 \times 10^{12} \text{ W/m}^2$, and (c) $4.92 \times 10^{12} \text{ W/m}^2$.

experiment was performed for varying intensities in order to analyze the dependence of the nonlinear absorption coefficient on the intensity of the laser beam. Materials with genuine 2PA possess nonlinear absorption coefficients independent of on-axis intensities, while materials with sequential 2PA demonstrate variation in nonlinear absorption coefficient with on-axis intensities. For analyzing this, the value of the nonlinear absorption coefficient (β) was extracted from the best theoretical fit obtained for experimental data obtained at different laser pulse energies. The value of β must be positive for the compounds to possess 2PA. For different pulse energies of 100, 150, and 200 μJ , the two-photon absorption coefficient of 7DMC was found as 0.65, 0.71, and $0.8 \times 10^{-10} \text{ m/W}$ respectively. So, the positive value of β shows the occurrence of 2PA in 7DMC. The value of β was observed to increase with the increase in the laser intensity and it represents that the 7DMC exhibits sequential two-photon absorption (one-photon absorption followed by excited state absorption). The simulated and experimental absorption pattern of 7DMC reveals the existence of $\pi-\pi^*$ transition with absorption maxima at 370 nm. This $\pi-\pi^*$ transition provides the possibility for the occurrence of two-photon absorption (2PA) [50]. Furthermore, efforts were made to employ the 7DMC as a utility material for laser safety devices. The OL behavior of 7DMC was estimated by plotting the OL graph (Fig. 8). The OL graph was also plotted for the same three intensities as taken for Z-Scan. The observed nonlinear pattern extracted from open aperture data symbolizes the occurrence of OL activity in the 7DMC sample. Here the normalized transmittance undergoes a gradual decrement with the increasing value of input laser fluence. From the OL graph, the OL threshold was also found to be decreased to 2.67, 2.41, and $2.04 \times 10^{13} \text{ W/m}^2$ for a pulse energy of 100, 150, and 200 μJ respectively (Fig. 9). The decrement in the OL threshold with increasing pulse energy validates the reinforcement of the OL behavior of 7DMC. Thus, the Z-Scan and OL analysis reveals the potential characteristics of 7DMC to be used as NLO and OL material. To make it a fair comparison and to support the present study, the optical limiting threshold of 7DMC was compared with some reference compounds like *para*-aminobenzoic acid ($2.24 \times 10^{13} \text{ W/m}^2$) [51], L-phenylalanine-benzoic acid ($6.5 \times 10^{13} \text{ W/m}^2$) [52], Benzothiazole pyrazole ($8.5982 \times 10^{13} \text{ W/m}^2$) [53], gold nanoparticles ($1.2 \times 10^{13} \text{ W/m}^2$) [54], C_{70} , C_{76} , C_{78} , and C_{84} fullerene ($2 \times 10^{13} \text{ W/m}^2$) [55,56], etc.

4. Conclusion

The quantum chemical calculations using DFT were performed for a coumarin derivative 7DMC. The band gap, spectroscopic calculations, and DFT equations were used to bring the reactivity of the 7DMC. As per the computational results, the experiments were further performed with the solution of the coumarin derivative 7DMC in DMF. The band gap obtained by simulation (3.691 eV) was found nearly close to the experimentally obtained band gap (3.68 eV). The other global and local reactivity descriptors were found to give promising values showing

intramolecular interactions. The charge distribution variation was found between the 1O, 2O, and 3N atoms and was validated by the potential and Hirshfeld's surfaces. The experimental UV-Vis and FT-IR spectra also coincided with the simulation results. Moreover, the UV-Vis spectra gave evidence of the transitions occurring mainly due to the $\pi-\pi^*$ transitions. The vibrational peaks were found with high IR intensity for the nitrogen and oxygen atoms. These high-intensity modes give chances of high polarizability of 7DMC. This was also verified by the NLO parameters. Finally, the experimental Z-Scan results were favorable enough to verify the NLO responses of 7DMC. The positive and increasing value of β with increasing intensity reveals the occurrence of sequential 2PA in 7DMC during the Z-scan experiment. Therefore, according to all the above-explained responses, it can be concluded that 7DMC has strong NLO characteristics and is a strong candidate for different NLO applications.

Ethical approval

Give my consent for the publication of identifiable details, which include data and pictures to be published in the journal.

Funding

S. Lakhera and M. Rana thank Uttarakhand Science Education and Research Centre (USERC), Department of Information and Science Technology, Government of Uttarakhand, for financial support through an R&D Research Project (Project no: USERC/2023-24/190).

CRediT authorship contribution statement

Shradha Lakhera: Visualization, Validation, Software, Investigation, Data curation, Conceptualization. **Kamal Devlal:** Writing – review & editing, Conceptualization. **Meenakshi Rana:** Writing – review & editing, Supervision, Methodology, Conceptualization. **N. Kanagathara:** Software, Data curation. **A. Dhanusha:** Resources, Investigation. **T.C. Sabari Girisun:** Investigation, Resources, Supervision, Visualization. **Shruti Sharma:** Resources, Investigation. **Papia Chowdhury:** Visualization, Supervision, Resources.

Declaration of Competing Interest

The authors declare that they have no known competing financial interests or personal relationships that could have appeared to influence the work reported in this paper.

Data availability

No data was used for the research described in the article.

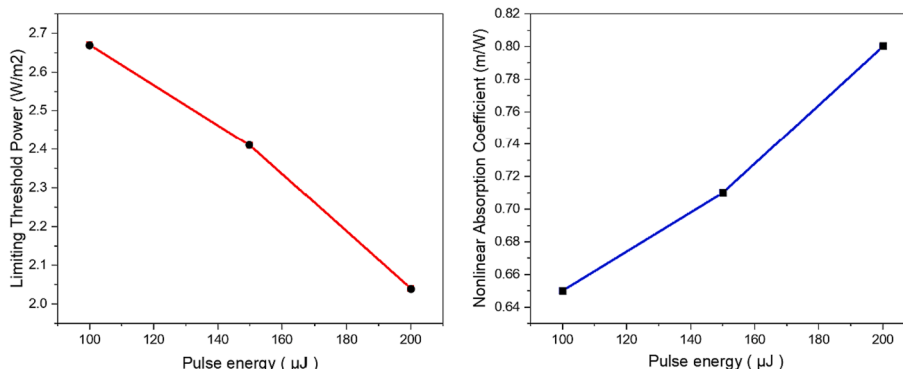


Fig. 9. Optical limiting threshold power of 7DMC vs. pulse energy of the incident laser in DMF.

Appendix A. Supplementary data

Supplementary data to this article can be found online at <https://doi.org/10.1016/j.jphotochem.2023.115216>.

References

- [1] A. Porfirev, S. Khonina, A. Kuchmizhak, Light–matter interaction empowered by orbital angular momentum: Control of matter at the micro- and nanoscale, *Prog. Quantum Electron.* 88 (2023), 100459, <https://doi.org/10.1016/j.pquantelec.2023.100459>.
- [2] S. Lakhera, K. Devlal, M. Rana, I. Celik, Study of nonlinear optical responses of phytochemicals of *Clitoria ternatea* by quantum mechanical approach and investigation of their anti-Alzheimer activity with in silico approach, *Struct. Chem.* (2022), <https://doi.org/10.1007/s11224-022-01981-5>.
- [3] S. Jinno, M. Kanasaki, T. Asai, et al., Laser-driven multi-MeV high-purity proton acceleration via anisotropic ambipolar expansion of micron-scale hydrogen clusters, *Sci. Rep.* 12 (2022) 16753, <https://doi.org/10.1038/s41598-022-18710-x>.
- [4] H. Alyar, A review on nonlinear optical properties of donor-acceptor derivatives of naphthalene and Azanaphthelene, *Rev. Adv. Mater. Sci.* 34 (2013) 79–87.
- [5] M.U. Khan, M. Khalid, R.A. Khera, M.N. Akhtar, A. Abbas, M.F. Rehman, A.A. C. Braga, M.M. Alam, M. Imran, Y. Wang, C. Lu, Influence of acceptor tethering on the performance of nonlinear optical properties for pyrene-based materials with A- π -D- π -D architecture, *Arab. J. Chem.* 15 (3) (2022), 103673, <https://doi.org/10.1016/j.arabjch.2021.103673>.
- [6] K. Jayakrishnan, A. Joseph, J. Bhattathiripad, M.T. Ramesan, K. Chandrasekharan, N.K.S. Narendran, Reverse saturable absorption studies in polymerized indole – Effect of polymerization in the phenomenal enhancement of third order optical nonlinearity, *Opt. Mater.* 54 (2016) 252–261, <https://doi.org/10.1016/j.optmat.2016.02.041>.
- [7] S. Lakhera, K. Devlal, A. Ghosh, M. Rana, In silico investigation of phytoconstituents of medicinal herb ‘Piper Longum’ against SARS-CoV-2 by molecular docking and molecular dynamics analysis, *Results in Chemistry.* 3 (2021), 100199, <https://doi.org/10.1016/j.rechem.2021.100199>.
- [8] M. Rana, N. Singla, A. Chatterjee, A. Shukla, P. Chowdhury, Investigation of nonlinear optical (NLO) properties by charge transfer contributions of amine functionalized tetraphenylethylene, *Opt. Mater.* 62 (2016) 80–89, <https://doi.org/10.1016/j.optmat.2016.09.043>.
- [9] M. Rana, P. Chowdhury, Effects of hydrogen bonding between pyrrole-2-carboxaldehyde and nearest polar and nonpolar environment, *Spectrochim. Acta - a: Mol. Biomol.* 185 (2017) 198–206, <https://doi.org/10.1016/j.saa.2017.05.050>.
- [10] S. Lakhera, M. Rana, K. Devlal, Theoretical study on spectral and optical properties of essential amino acids: a comparative study, *Opt. Quant. Electron.* 54 (2022) 714, <https://doi.org/10.1007/s11082-022-04118-4>.
- [11] A. Gowda, L. Jacob, A. Patra, A. George, R. Philip, S. Kumar, Synthesis, mesomorphic properties and nonlinear optical studies of alkyl and alkoxy phenylacetylene containing phenazine fused extended triphenylene discotic liquid crystalline dyes, *Dyes Pigm.* 160 (2019) 128–135, <https://doi.org/10.1016/j.dyepig.2018.07.052>.
- [12] S. Mandal, G.R. Kandregula, V.N.B. Tokala, A computational investigation of the influence of acceptor moieties on photovoltaic performances and adsorption onto the TiO₂ surface in triphenylamine-based dyes for DSSC application, *J. Photochem. Photobiol. A Chem.* (2020), <https://doi.org/10.1016/j.jphotochem.2020.112745>.
- [13] M. Hachi, S.E. Khattabi, A. Fitri, A.T. Benjelloun, M. Benzakour, M. Mcharfi, M. Hamidi, M. Bouachrine, FT and TD-DFT studies of the pi-bridge influence on the photovoltaic properties of dyes based on thieno[2,3-b]indole, *J. Mater. Environ. Sci.* 9 (4) (2018) 1200–1211, <https://doi.org/10.26872/jmes.2017.9.4.132>.
- [14] J. Suryapratap, N.G. Sharma, Deep-red/NIR emitting coumarin derivatives - Synthesis, photophysical properties, and biological applications, *Dyes Pigm.* 202 (2022), 110306, <https://doi.org/10.1016/j.dyepig.2022.110306>.
- [15] N. Chanda, S. Gonuguntla, S.K. Verma, A.K. Basak, Y. Soujanya, M. Ahmadipour, S. Bojja, U. Pal, Shedding light on small molecule coumarin dyes for efficient photocatalytic hydrogen evolution, *Int. J. Hydrog. Energy.* (2022), <https://doi.org/10.1016/j.ijhydene.2022.09.108>.
- [16] A. Pal, M. Karmakar, S.R. Bhatta, A. Thakur, A detailed insight into anion sensing based on intramolecular charge transfer (ICT) mechanism: A comprehensive review of the years 2016 to 2021, *Coord. Chem. Rev.* 448 (2021), 214167, <https://doi.org/10.1016/j.ccr.2021.214167>.
- [17] N.N. Ayare, M.C. Sreenath, S. Chitrabalam, I.H. Joe, N. Sekar, NLO characteristics of D- π -A coumarin-thiophene bridged azo dyes by Z-scan and DFT methods, *Mol. Phys.* (2019), <https://doi.org/10.1080/00268976.2019.1662127>.
- [18] M. Rajeshirke, M.C. Sreenath, S. Chitrabalam, I.H. Joe, N. Sekar, Enhancement of NLO Properties in OBO Fluorophores Derived From Carbazole-Coumarin Chalcones Containing Carboxylic Acid at the N-Alky Terminal End, *J. Phys. Chem. C* (2018), <https://doi.org/10.1021/acs.jpcc.8b02937>.
- [19] K.N. Sharafudeen, A. Adithya, S. Vijayakumar, P. Sudheesh, B. Kalluraya, K. Chandrasekharan, Multiphoton absorption process and self-focusing effect in coumarin derivative doped PMMA films by z-scan and optical limiting studies, *Curr. Appl Phys.* 11 (4) (2011) 1089–1093, <https://doi.org/10.1016/j.cap.2011.02.001>.
- [20] K.N.C. Prathap, N.K. Lokanath, Three novel coumarin benzenesulfonylhydrazide hybrids: Synthesis, characterization, crystal structure, Hirshfeld surface, DFT and NBO studies, *J. Mol. Struct.* (2018), <https://doi.org/10.1016/j.molstruc.2018.06.022>.
- [21] M.M. Raikwar, K.C. Avhad, M. Varghese, E. Mathew, I.H. Joe, N. Sekar, D- π -A- π -D coumarin hybrids derived from arylamine donors: DFT and Z-scan studies, *Opt. Mat.* 92 (2019) 100–110, <https://doi.org/10.1016/j.optmat.2019.04.011>.
- [22] N. Arif, Z. Shafiq, S. Noureen, M. Khalid, A. Ashraf, M. Yaqub, S. Irshad, M. U. Khan, M. Nadeem Arshad, A.A.C. Braga, A.H. Ragabh, S.R.A. Mhyawii, Synthesis, spectroscopic, SC-XRD/DFT and nonlinear optical (NLO) properties of chromene derivatives, *RSC Adv.* 13 (2023) 464–477, <https://doi.org/10.1039/D2RA07134G>.
- [23] N. Ben Azaza, S. Elleuch, M. Rasheed, D. Gindre, S. Abid, R. Barille, Y. Abid, H. Ammar, 3-(p-nitrophenyl)Coumarin derivatives: Synthesis, linear and nonlinear optical properties, *Opt. Mater.* 96 (2019), 109328, <https://doi.org/10.1016/j.optmat.2019.109328>.
- [24] M. J. Frisch, G. W. Trucks, H. B. Schlegel, et al, Gaussian 09, Revision B. 01, Gaussian Inc., Wallingford CT. 121 (2009) 150-166.
- [25] A.D. Becke, Density-functional thermochemistry. V. Systematic optimization of exchange-correlation functionals, *J. Chem. Phys.* 107 (1997) 8554–8560, <https://doi.org/10.1063/1.475007>.
- [26] N.M. O’Boyle, A.L. Tenderholt, K.M. Langner, *J. Comp. Chem.* 29 (2008) 839–845.
- [27] S. Lakhera, M. Rana, K. Devlal, Investigation of the electronic and optical activity of halogen-substituted 2-dinitrotoluene by density functional theory, *Opt. Quant. Electron.* 55 (2023) 292, <https://doi.org/10.1007/s11082-023-04569-3>.
- [28] S. Lakhera, M. Rana, K. Devlal, Investigation of Nonlinear Optical Responses of Organic Derivative of Imidazole: Imidazole-2-carboxaldehyde, *IJMR.* 114 (7–8) (2023) 555–563, <https://doi.org/10.1515/ijmr-2021-8649>.
- [29] N. Kanagathara, F. MaryAnjalin, V. Ravagendran, D. Dhanasekaran, R. Usha, R. Gowri Shankar Rao, M.K. Marchewka, Experimental and Theoretical (DFT) investigation of Crystallographic, Spectroscopic, and Hirshfeld surface analysis of anilinium arsenate, *J. Mol. Struct.* (2020), <https://doi.org/10.1016/j.molstruc.2020.128965>.
- [30] M. Rana, N. Singla, A. Pathak, A. Dhanya, C. Narayana, P. Chowdhury, Vibrational-electronic properties of intra/inter molecular hydrogen bonded heterocyclic dimer: An experimental and theoretical study of pyrrole-2-carboxaldehyde, *Vib. Spectrosc.* 89 (2017) 16–25, <https://doi.org/10.1016/j.vibspec.2016.12.003>.
- [31] J. Singh, Electronic processes in amorphous semiconductors, *J. Mater. Sci. Mater. Electron.* 14 (2003) 171–186, <https://doi.org/10.1023/A:1022310108978>.
- [32] S. Lakhera, K. Devlal, M. Rana, V. Dhuliya, Quantum Mechanical Study of Three Aromatic Bioactive Fatty Alcohol Compounds with Nonlinear Optical and Potential Light-Harvesting Properties, *Opt. Mat.* 129 (2022), 112476, <https://doi.org/10.1016/j.optmat.2022.112476>.
- [33] A. Bimoussa, A. Oubella, M.E. Hachim, M. Fawzi, M.Y.A. Itto, O. Mentre, E. M. Ketatni, L. Bahsis, H. Morjani, A. Auhmani, New enamione sesquiterpene: TiCl₄-catalyzed synthesis, spectral characterization, crystal structure, Hirshfeld surface analysis, DFT studies and cytotoxic activity, *J. Mol. Struct.* 1241 (2021), 130622, <https://doi.org/10.1016/j.molstruc.2021.130622>.
- [34] Y. Li, J.N.S. Evans, The Fukui Function: A Key Concept Linking Frontier Molecular Orbital Theory and the Hard-Soft- Acid-Base Principle, *J. Am. Chem.* 117 (1995) 7756–7759, <https://doi.org/10.1021/ja00134a021>.
- [35] Q.S. Obu, H. Louis, J.O. Odey, I.J. Eko, S. Abdullahi, T.N. Ntui, O.E. Offiong, Synthesis, spectra (FT-IR, NMR) investigations, DFT study, in silico ADMET and Molecular docking analysis of 2-amino-4-(4-aminophenyl)thiophene-3-carbonitrile as a potential anti-tubercular agent, *J. Mol. Struct.* 1244 (2021), 130880, <https://doi.org/10.1016/j.molstruc.2021.130880>.
- [36] A. Bendjeddou, T. Abbas, A. K. Gouasmia, D. Villemin, Molecular Structure, HOMO-LUMO, MEP and Fukui Function Analysis of Some TTF-donor Substituted Molecules Using DFT (B3LYP) Calculations. *IJPAC.* 12(1) 920161-9. <https://doi.org/10.9734/IJPAC/2016/27066>.
- [37] V. Pilepić, S. Uršić, Nucleophilic reactivity of the nitroso group. Fukui function DFT calculations for nitrosobenzene and 2-methyl-2-nitrosopropane, *J. Mol. Struct. (Theochem)* 538 (1–3) (2001) 41–49, [https://doi.org/10.1016/S0166-1280\(00\)00642-4](https://doi.org/10.1016/S0166-1280(00)00642-4).
- [38] S. Lakhera, M. Rana, K. Devlal, Influence of Adsorption of Gold and Silver Nanoclusters on Structural, Electronic, and Nonlinear optical properties of Pentacene-5, 12-dione: A DFT study, *Opt. Quant. Electron.* 55 (2023) 178, <https://doi.org/10.1007/s11082-022-04422-z>.
- [39] T. Hema, P. Bhatt, C. Arya, H. Dhondiyal, K. Tiwari, Devlal, Structural and vibrational study of molecular interaction in a ternary liquid mixture of benzylamine, ethanol and benzene, *Struct. Chem.* (2021), <https://doi.org/10.121203/rs.3.rs-649250/v1>.
- [40] S. Lakhera, K. Devlal, M. Rana, V. Dhuliya, Computational study of non-linear optical and electrical properties of 1,3-dinitropropene, *Opt. Quant. Electron.* 55 (2023) 85, <https://doi.org/10.1007/s11082-022-04371-7>.
- [41] Z. Lin, Z. Wang, C. Chen, M.H. Lee, Mechanism of linear and nonlinear optical effects of KDP and urea crystals Citation, *J. Chem. Phys.* 118 (2003) 2349, <https://doi.org/10.1063/1.1533734>.
- [42] S. Lakhera, M. Rana, K. Devlal, N. Kanagathara, J. Janczak, Photovoltaic Characteristics of Organic Heterocyclic 2,9-dimethyl Quinacridone in Different Solvents Using DFT Approach, *J. Photochem. Photobiol. A Chem.* 114664 (2023), <https://doi.org/10.1016/j.jphotochem.2023.114664>.
- [43] S. Lakhera, K. Devlal, A. Ghosh, M. Rana, Modelling the DFT structural and reactivity study of feverfew and evaluation of its potential antiviral activity against COVID-19 using molecular docking and MD simulations, *Chem. Pap.* (2022), <https://doi.org/10.1007/s11696-022-02067-6>.

- [44] M. Rana, A. Jain, V. Rani, P. Chowdhury, Glutathione capped core/shell CdSeS/ZnS quantum dots as a medical imaging tool for cancer cells, *Inorg. Chem. Commun.* 112 (2020), 107723, <https://doi.org/10.1016/j.inoche.2019.107723>.
- [45] O.A. Sapozhnikov, J.A.G. Juárez, K.F. Graff, M. Lucas, High-intensity ultrasonic waves in fluids: Nonlinear propagation and effects, in: Woodhead Publishing Series in Electronic and Optical Materials, Power Ultrasonics, (Second Edition), Woodhead Publishing, 2023, pp. 7–22, <https://doi.org/10.1016/B978-0-12-820254-8.00014-2>.
- [46] S. Lakhera, M. Rana, K. Devlal, I. Celik, R. Yadav, A comprehensive exploration of pharmacological properties, bioactivities and inhibitory potentiality of luteolin from *Tridax procumbens* as anticancer drug by in-silico approach, *Struct. Chem.* (2022), <https://doi.org/10.1007/s11224-022-01882-7>.
- [47] S. Lakhera, K. Devlal, M. Rana, V. Dhuliya, N. Pandey, Non-Linear Optical Behavior of 2,9-Dimethylquinacridone with Adsorbed Gold and Silver Nanoclusters, *Optik* (2023), 170983, <https://doi.org/10.1016/j.jjleo.2023.170983>.
- [48] S. Adhikari, T. Kar, Experimental and theoretical studies on physicochemical properties of l-leucine nitrate—a probable nonlinear optical material, *J. Cryst. Growth* 356 (2012) 4–9, <https://doi.org/10.1016/j.jcrysgro.2012.07.008>.
- [49] T.C. Sabari Girisun, S. Dhanuskodi Nonlinear optical susceptibilities of diglycinyll thiourea for frequency conversion and optical limiting applications a Chemical Physics Letters 491 (2010) 248–253. <https://doi.org/10.1016/j.cplett.2010.04.014>.
- [50] A. Pramothkumara, N. Senthilkumarb, R. Mary Jenilac, M. Durairaj, T.C. Sabari Girisund, I.V. Pothehera, A study on the electrical, magnetic and optical limiting behaviour of Pure and Cd-Fe co-doped CuO NPs, *J. Alloy. Compd.* 878 (2021), 160332, <https://doi.org/10.1016/j.jallcom.2021.160332>.
- [51] S. Lakhera, M. Rana, K. Devlal, S. Sharma, P. Chowdhury, V. Dhuliya, S. Panwar, L. P. Purohit, A. Dhanusha, T.C. Girisun, Exploring the Nonlinear Optical Limiting Activity of Para-Aminobenzoic Acid by Experimental and Dft Approach, *J Photochem. Photobiol. A* (2023), 114987, <https://doi.org/10.1016/j.jphotochem.2023.114987>.
- [52] D.S. Madhu, S. Devasenan, et al., Extraction of Natural Pigment Curcumin from *Curcuma Longa*: Spectral, DFT, Third-order Nonlinear Optical and Optical Limiting Study, *J. Fluoresc.* (2023), <https://doi.org/10.1007/s10895-023-03421-x>.
- [53] A.G. Pramod, Y.F. Nadaf, C.G. Renuka, C.G.Synthesis, photophysical, quantum chemical investigation, linear and non-linear optical properties of coumarin derivative: Optoelectronic and optical limiting application, *Spectrochim. Acta - a: Mol. Biomol. Spectrosc.* 223 (2019), 117288, <https://doi.org/10.1016/j.saa.2019.117288>.
- [54] C.W. Ghanavatkar, V.R. Mishra, N. Sekar, E. Mathew, S.S. Thomas, I.H. Joe, Benzothiazole pyrazole containing emissive azo dyes decorated with ES IPT core: Linear and non linear optical properties, Z scan, optical limiting, laser damage threshold with comparative DFT studies, *J. Mol. Struct.* 1203 (2020), 127401, <https://doi.org/10.1016/j.molstruc.2019.127401>.
- [55] Y. Gündoğdu, Third-order nonlinear optical properties of fullerene C60 in organic solvents using femtosecond laser z-scan, *Indian J. Phys.* 97 (2023) 915–922, <https://doi.org/10.1007/s12648-023-02612-3>.
- [56] D. Vincent, J. Cruickshank, Optical limiting with C60 and other fullerenes, *Optica Publishing Group.* 36 (30) (1997) 7794–7798, <https://doi.org/10.1364/AO.36.007794>.